京都大学防災研究所年報 第40号 B-1 平成9年4月
Annuals of Disas. Prev. Res. Inst., Kyoto Univ., No. 40 B-1, 1997

Strength of Gneiss in the Lishan Landslide Slope under Confining Pressure

Mitsuhiko SHIMADA

Synopsis

Two gneisses from the Lishan landslide slope were studied experimentally, for understanding the mechanism of Lishan landslide. These two rocks are situated faced to a possible potential sliding surface, upper bedrock LGNA and lower one LGNB. LGNA has an extensive anisotropic structure of mylonitized foliation, while LGNB is isotropic. The compressive strength and the residual strength of these rocks were measured at room temperature under a confining pressure up to 40 MPa. Both rocks have the same compressive and residual strengths and the same pressure dependencies. The compressive strength for the LGNA sample with foliation oriented at 30° to the compressive stress direction is close to the residual strength. LGNA has higher porosity than LGNB. These results suggest that a high pore pressure could be possibly formed in the boundary between these bedrocks and the boundary could form a potential sliding surface.

Keywords: triaxial testing; gneiss; strength; landslide; Lishan, China

1. Introduction

Landslide in Lishan (Huanqing Palace), Xi'an, Shaanxi, China (Fig. 1), has been extensively investigated by the joint research program between China and Japan (e.g., Sassa, 1994; Sassa and Xie, 1994). Two possible mechanisms of the Lishan landslide are proposed: sliding by surface layer creep by Lin (1989) and sliding by bedrock creep by Sassa et al. (1994).

The latter idea includes the fault motion in Precambrian gneiss (cf. Fig. 2). The rocks faced to the fault plane that would be regarded as a possible potential sliding surface, are different each other in apparent features. However, mechanical properties of these rocks have not been known, although the geological structure associated with fault planes and the joint system have been studied (Xie, et al., 1994; Kitagawa, 1997). Knowledge of mechanical properties of these rocks is indispensable for our understanding of the mechanism of landslide.

Two Precambrian gneisses that are faced to the fault plane were sampled in the 1994 Japan-China

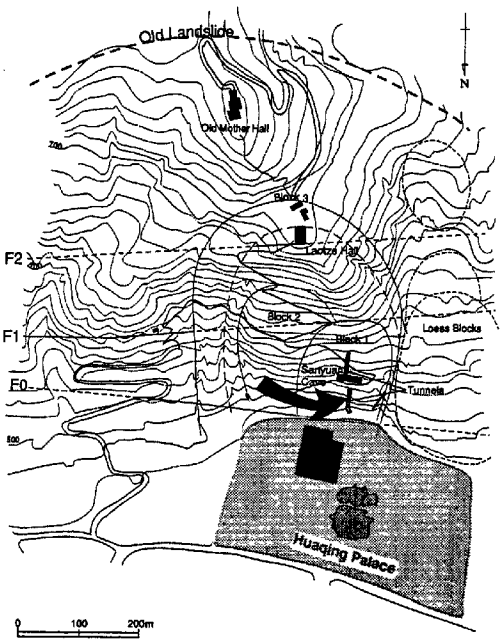

Fig. 1 Plan of the Lishan landslide slope (Sassa and Xie, 1994) and the location of the lower observation tunnel (arrow).

Joint Research Project on Lishan Landslide. Here, we report the results of triaxial testing on the sampled gneiss rock specimens that include the compressive strength and the residual strength up to a confining pressure of 40 MPa at room temperature. A possible mechanism of sliding between both bedrocks is also discussed.

2. Rock Specimens

Rock specimens were sampled at two points in the lower observation tunnel excavated in the Lishan slope (Fig. 1). One is from the upper bedrock of a fault plane that is considered to be a possible sliding surface, designated as LGNA, and the other is from the lower bedrock, designated as LGNB. The geological cross-sectional view of the Lishan slope and the sampled points are shown in Fig. 2. Figure 3 shows the geological structure in the lower observation tunnel and the sampling sites. LGNA was sampled from the east wall of the tunnel at 7 m from the entrance, and LGNB was from the west wall

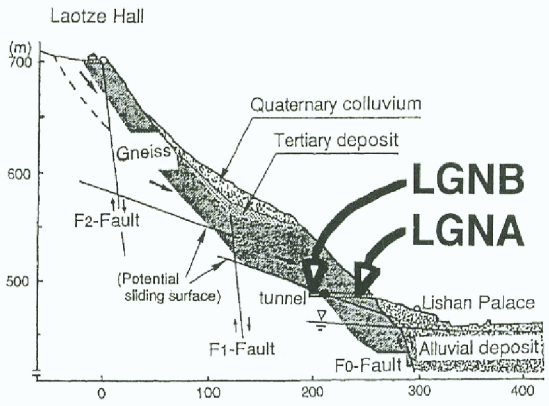

Fig. 2 The geological cross-sectional view of the Lishan slope (Sassa et al. 1994) and the points where two rock specimens, LGNA and LGNB were sampled in the lower observation tunnel.

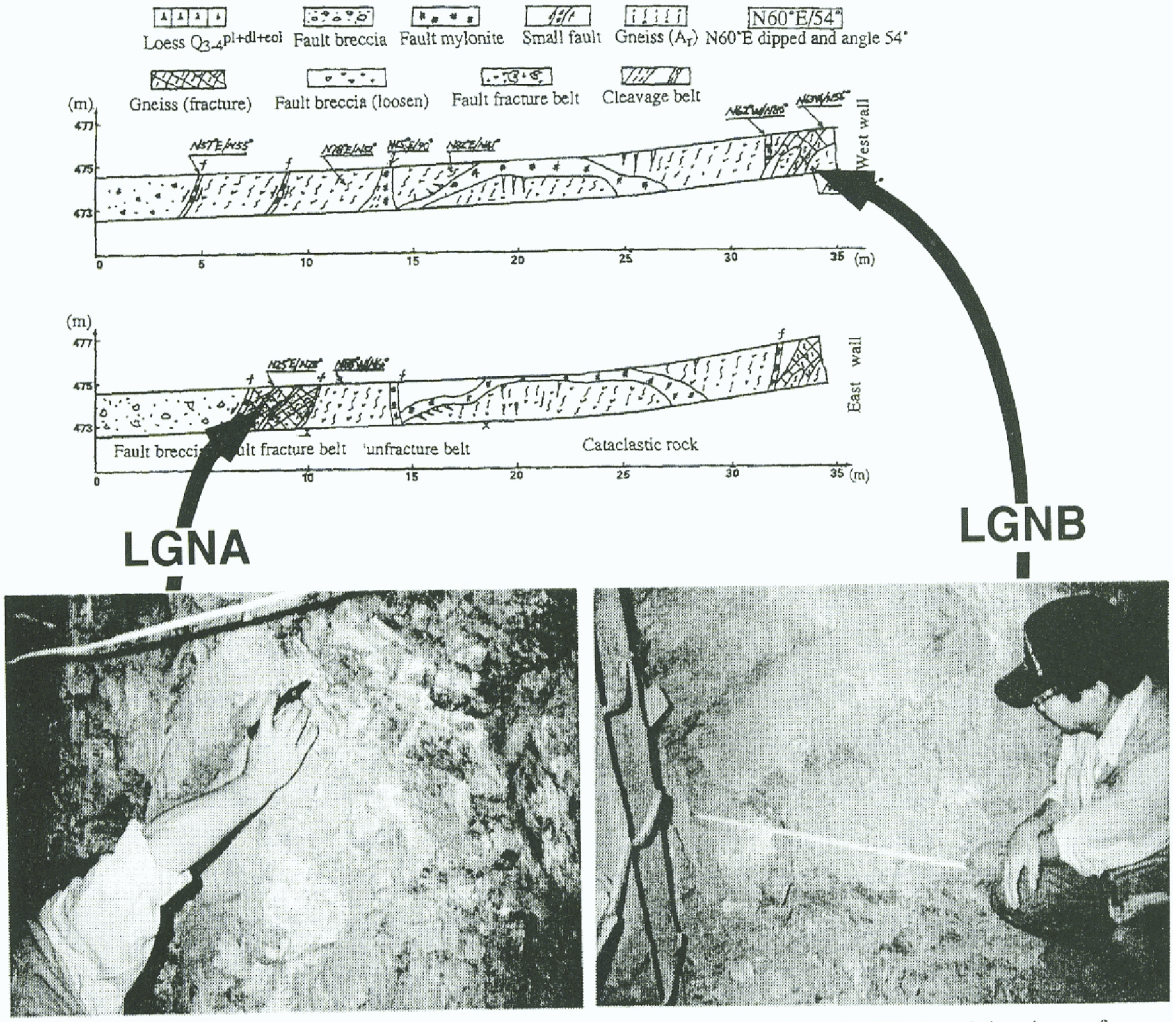

Fig. 3 The geological structure in the lower observation tunnel (Xie et al., 1994) and the views of sampling sites.

at the end of the tunnel.

Both rocks are Precambrian mylonitized pelitic gneisses. An anisotropic structure of mylonitized foliation is developed in LGNA along which macroscopic cracks are formed (dip 54° N, see the left photograph in Fig. 3). LGNB is macroscopically isotropic. The typical photomicrographs are shown in Fig. 4. Their petrological characteristics are as follows (Kitagawa, personal communication). Very few constitutive minerals of source rock remain, which are quartz, potassium feldspar, garnet, biotite, muscovite and bearing minerals such as apatite and zircon. Recrystallized minerals by the metamorphism, which is possibly in greenschist facies, are quartz, sericite, muscovite and chlorite. Most of crystalline axes in quartz are oriented at a fixed direction by the metamorphism. Most biotite of source rock are altered to muscovite. LGNA is less mylonitized than LGNB and includes more minerals of source rock. Veined calcite and zeorite are included in LGNA, which are considered to be formed by later hydrothermal processes.

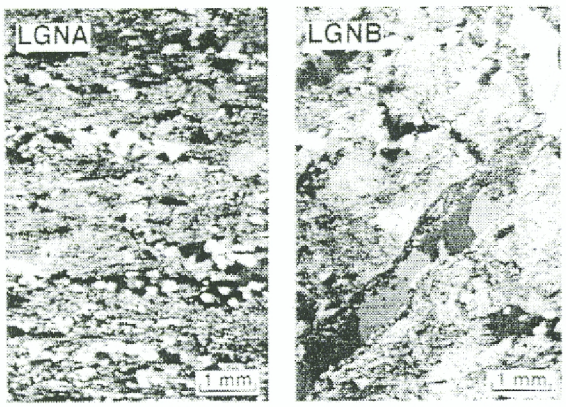

Fig. 4 Typical photomicrographs of LGNA (left) and LGNB (right). Crossed nicols.

The results of modal analyses of these two gneisses are listed with grain sizes in Table 1. Their density and porosity were measured, being 2.735 Mg/m^3 and 3.28% for LGNA, respectively, and 2.720 Mg/m^3 and 1.05% for LGNB, respectively, which are also listed in Table 1.

3. Experimental Method

For triaxial testing, a cylindrical rock sample

Table 1 Description of two rock specimens from Lishan, Shaanxi, China

Rock (mode, %)[1)]	Grain size[1)] (mm)	Density[2)] (Mg/m^3)	Porosity[3)]
LGNA mylonitized pelitic gneiss, (qz: 48.8; or: 12.1, pl: 3.3, gt: 0.4, src: 21.2, mu:9.9, bi: 4.2)	qz: 0.1~0.3 or: 0.3~1.1 pl: 0.3~1.0 gt: 0.05~0.2 src: (0.013×0.15) ~(0.005×0.075) mu: (0.025×0.375) ~(0.1×0.6) bi: (0.05×0.1)	ρ = 2.735±0.001 ρ_a= 2.6756±0.0004 ρ_B= 2.6450±0.0001	P_T= 3.28±0.05% P_a= 1.15±0.01%
LGNB mylonitized pelitic gneiss (more mylonitized than LGNA), (qz: 39.0; or: 19.6, pl: 0.1, gt: 0.2, src: 25.9, mu:9.0, bi: 0.2, cc: 1.9, ze: 3.4, chl: 0.7)	qz: 0.07~1.0 or: 0.7~1.0 src:(0.025×0.005) ~(0.013×0.25) mu: (0.02×0.007) ~(0.1×0.3) cc: 0.5~1.0 ze: 0.013~0.075 chl: 0.4	ρ = 2.720±0.003 ρ_a= 2.7100±0.0002 ρ_B= 2.6915±0.0004	P_T= 1.05±0.01% P_a= 0.69±0.01%

1) qz = quartz; or = orthoclase; pl = plagioclase; gt = garnet; src = sericite; mu = muscovite; bi = biotite; cc = calcite; ze = zeorite; chl = chlorite.
2) ρ_a= apparent density; ρ_B= bulk density.
3) P_T= total porosity; P_a= apparent porosity.

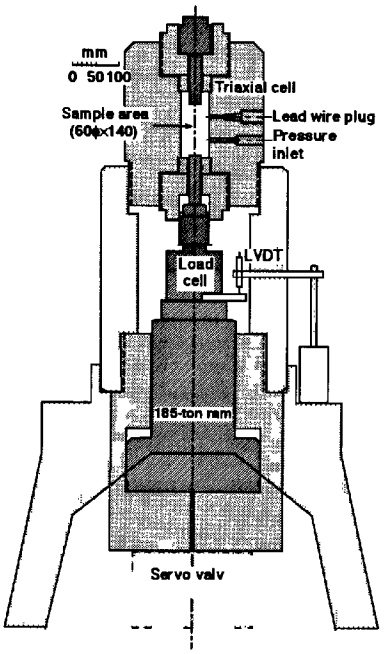

Fig. 5 Cross-sectional view of the conventional triaxial testing apparatus used in this study. Pumping system and a booster for confining pressure are not shown.

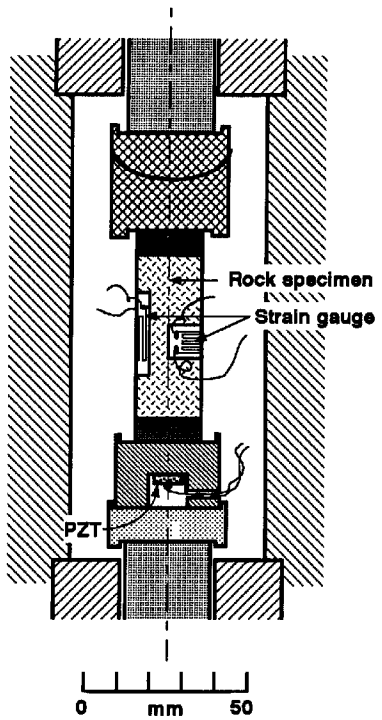

Fig. 6 The sample configuration in the sample area of the apparatus shown in Fig. 5.

was used of 20 mm in diameter and 50 mm in length, or of 18 mm in diameter and 36 mm in length. Three samples are prepared for LGNA according to mylonitized foliation, with foliation oriented at 90° to the compressive stress direction, at 30° and at 45°, which are designated as $LGNA_{\perp}$, $LGNA_{30}$, and $LGNA_{45}$, respectively. Each sample was dried in vacuum at 110°C for more than 24 hours. Two electrical resistance strain gauges were stuck on the surface of each cylindrical rock sample in axial and circumferential directions, by which axial strain ε_1 and circumferential strain ε_3 were measured, respectively. Then, each rock sample was jacketing with polyolefine heat-shrinkable tubing to prevent confining pressure transmitting oil from entering the rock.

Triaxial testing was conducted using a conventional apparatus with capability of generation of confining pressure up to 500 MPa. This apparatus was originally designed by Kiyama (1956), used for rock mechanics by Matsushima (1960), and has been thereafter modified in several parts, such as installation of a servo controlled system for axial loading (Yukutake, 1989). The cross-sectional view of the apparatus is shown in Fig. 5, and the sample configuration is shown in Fig. 6. Acoustic emission (AE) was measured by means of a piezoelectric transducer PZT (lead zirconate titanate, $Pb(Zr\cdot Ti)O_3$) fixed in the hollowed end piece of hardened steel (Fig. 6). The axial load was increased at a constant displacement rate of approximately 1×10^{-4} mm/s (corresponding to the axial strain rate of approximately 1×10^{-6} /s), which was servo-controlled through a LVDT (linear variable differential transformer) (Fig. 5).

Two series of triaxial tests were conducted. In the first series, conventional single-stage triaxial tests were performed at a fixed confining pressure. In each test, peak and residual (if possible) strengths were obtained. An example of stress-strain curve in a single-stage test is shown in Fig. 7, in which AE activity is also shown by the cumulative frequency of AE.

In the second series, the multi failure state triaxial tests (MFSTT) were conducted when peak stress was apparently detected (see, Kovári and Tisa, 1975; ISRM, 1983; Hossaini and Vutukuri, 1993). The aim of the MFSTT is to obtain several stress points of the failure envelope with one rock sample that has positive failure envelope, namely positive confining pressure dependency of the strength. The brief procedure is as follows according to Hossaini and Vutukuri (1993), of which example performed in this study is shown in Fig. 8. First, the confining

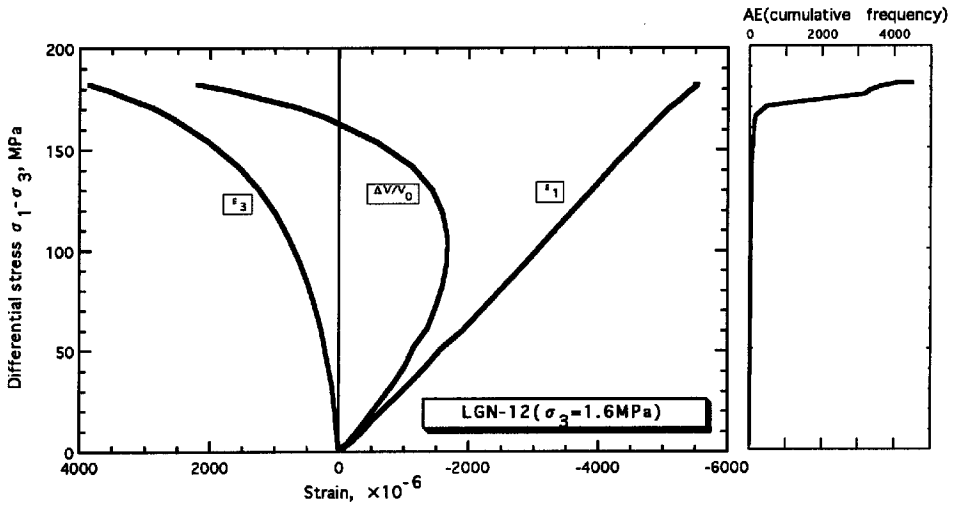

Fig. 7 An example of the stress-strain curve in the conventional single-stage triaxial test. ε_1 is the axial strain, ε_3 is the circumferential strain, and $\Delta V/V_0$ (= $\varepsilon_1 + 2\varepsilon_3$) is the volumetric strain.

pressure was increased to an expected value as low as possible. The axial load on the rock sample was then increased continuously at a constant strain rate. The onset of fracture was normally marked by the load remaining constant or decreasing slowly while deformation increased. In this study, observed AE activity was helpful to detect the onset of fracture (Fig. 8). As soon as a failure was observed from the load-displacement curve, the axial load was quickly put on hold and the confining pressure was increased to a next level. Then, the axial load was increased continuously with the same strain rate, and the peak stress was observed at the confining pressure. After all the peak stresses were obtained at different confining pressures, the confining pressure was reducedslowly to a certain level while the axial load was continuously applied. The load-displacement curve became flat after an initial sharp drop, then the residual stress was obtained. Afterwards the confining pressure was reduced slowly to another level and the

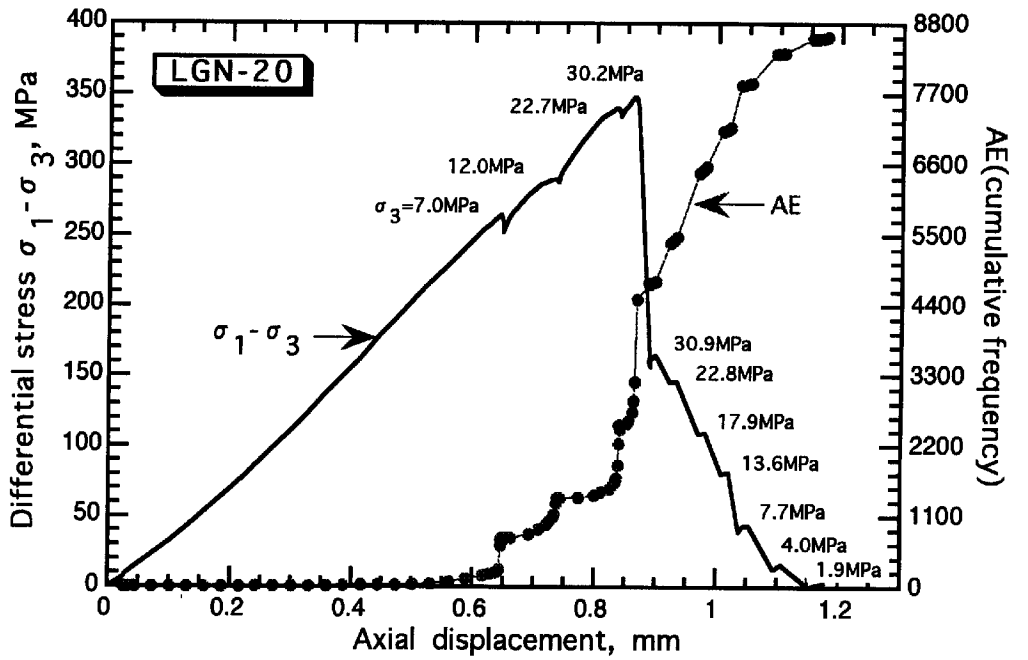

Fig. 8 An example of differential stress and AE activity as a function of axial displacement performed in the multi failure state triaxial test (MFSTT).

Table 2 Strength data of Lishan gneiss at room temperature

Run number	Confining pressure σ_3, MPa	Peak stress σ_1-σ_3, MPa	Residual stress σ_1-σ_3, MPa	Fracture angle	Normal stress σ_n, MPa	Shear stress τ, MPa	Comments
(Sample: $A_\perp$)[1]							
LGN-2	10.0±0.3	236.0±0.9		30°	69.0±3.6	102.2±2.1	other cracks at 20° and 40°
"	11.8±0.3		22.0±11.0	30°	17.3±2.8	9.5±4.8	"
LGN-5	3.3±2.1	230.8±1.2		20°	30.3±3.3	74.2±3.1	
LGN-7	0.1	166.4±0.4		20°	19.5±1.9	53.5±2.2	another crack at 20°
LGN-12	1.6±0.2	182.0±1.2		30°	47.1±2.8	78.8±1.7	
LGN-19	5.1±0.2	256.1±1.6		25°	50.8±3.5	98.1±2.9	MFSTT[2], other cracks at 30° and 10°
"	12.8±0.4	307.3±1.6		25°	67.7±4.2	117.7±3.5	"
"	13.5±0.4		16.5±1.8	25°	16.5±0.6	6.3±0.7	"
LGN-20	7.0±0.3	264.4±1.5		20°	37.9±3.0	85.0±3.6	MFSTT[2], other cracks at 30°, 40° and 45°
"	12.0±0.3	289.6±1.5		20°	45.9±3.3	93.1±3.9	"
"	22.7±0.1	340.2±1.5		20°	62.5±3.8	109.3±4.6	"
"	30.2±0.1	347.8±1.5		20°	70.8±3.9	111.8±4.7	"
"	30.9±0.1		162.4±2.8	20°	49.9±1.9	52.2±2.3	"
"	22.8±0.1		145.6±1.5	20°	39.9±1.6	46.8±2.0	"
"	17.9±0.1		108.9±1.5	20°	30.7±1.2	35.0±1.5	"
"	13.6±0.1		80.8±2.3	20°	23.1±1.0	26.0±1.3	"
"	7.7±0.1		43.4±1.5	20°	12.8±0.5	13.9±0.8	"
"	4.0±0.1		15.2±1.7	20°	5.7±0.3	4.9±0.6	"
"	1.9±0.1		1.9±1.6	20°	2.1±0.2	0.6±0.5	"
(Sample: A_{30})[1]							
LGN-14	2.3±0.2	78.1±1.3		30°	21.8±1.2	33.8±0.9	fractured along mylonite foliation
LGN-15	5.5±0.1	134.9±1.6		30°	39.2±2.1	58.4±1.4	"
(Sample: A_{45})[1]							
LGN-16	2.9±0.2	180.7±0.7		25°	35.2±2.4	69.2±2.1	another crack at 30°
LGN-17	5.6±0.2	179.5±2.6		30°	50.5±2.8	77.7±1.9	other cracks at 45° and 0°
(Sample: B)							
LGN-3	0.1	175.1±1.6		20°	20.5±2.0	56.3±2.4	
LGN-4	0.1	167.0±0.4		15°	11.2±1.5	41.8±2.5	
LGN-8	29.2±0.6	324.5±1.0		30°	110.3±5.0	140.5±2.9	another crack at 10°
"	29.6±0.1		160.9±4.8	30°	69.8±2.7	69.7±2.5	"

Table 2 Continued

Run number	Confining pressure σ_3, MPa	Peak stress σ_1-σ_3, MPa	Residual stress σ_1-σ_3, MPa	Fracture angle	Normal stress σ_n, MPa	Shear stress τ, MPa	Comments
(Sample: B)							
LGN-13	7.6±0.2	290.1±2.3		30°	80.1±4.4	125.6±2.7	
"	10.0±0.2		61.9±2.3	30°	25.5±1.1	26.8±1.1	
LGN-18	5.6±0.3	232.2±4.5		30°	63.6±3.7	100.5±2.8	MFSTT[2], other cracks at 45° and 25°
"	16.8±0.3	310.2±4.5		30°	94.3±4.8	134.3±3.3	"
"	25.8±0.1	361.6±4.5		30°	116.2±5.6	156.6±3.7	"
"	38.2±0.4	412.2±4.5		30°	141.2±6.4	178.5±4.1	"
"	38.6±0.1		334.0±4.6	30°	122.1±5.2	144.6±3.5	"
"	20.0±0.1		167.8±4.5	30°	62.0±2.8	72.7±2.4	"
"	13.1±0.3		112.4±4.5	30°	41.2±2.1	48.7±2.2	"
"	8.6±0.1		71.9±4.5	30°	26.5±1.6	31.1±2.0	"
"	3.0±0.1		9.0±4.5	30°	5.2±1.1	3.9±2.0	"

1) $A_\perp$, A_{30} and A_{45} are the samples with mylonitized foliation oriented at 90°, 30° and 45° to the compressive stress direction, respectively.
2) MFSTT: Multi failure state triaxial test.

corresponding residual stress was similarly obtained, until all the residual stresses of the rock sample at different confining pressure were determined.

The validity of MFSTT to determine the peak strength and the residual strength of rocks was ascertained by Hossaini and Vutukuri (1993). However, it is assumed that the fracture mechanism should not be changed during MFSTT in each confining pressure, which means that the fracture process, or the fracture nucleation process is identical for each confining pressure, unlike such as suggested by Shimada and Cho (1990). Since this study was conducted in the lower level of confining pressure at which such a change never occurs, the results of two series, conventional single-stage tests and MFSTTs, are discussed together.

4. Experimental Results and Discussion

Experimental results are summarized in Table 2. Peak and residual strengths as a function of confining pressure are shown in Fig. 9 (a for LGNA and b for LGNB).

For LGNA, the peak strength is the highest for $LGNA_\perp$, middle for $LGNA_{45}$, and the lowest for $LGNA_{30}$, although data are limited in the latter two cases. The peak strengths of $LGNA_\perp$ are identical to those for LGNB in MFSTT as well as the single-stage tests for the whole range of confining pressure. The compressive strength of rocks is known to be well represented empirically by a power law of confining pressure at moderate confining pressures up to 1000 MPa. Ohnaka (1973) gave the relationship:

$$C/C_0 = 1 + K\,(\sigma_3/C_0)^n$$

where C_0 is the uniaxial compressive strength, C is the strength at confining pressure σ_3, and K and n are constants depending on rock type. Applying this relationship to the studied gneiss with C_0 = 169.5 ±1.7 MPa, K and n are 4.34 and 0.72, respectively, which is shown by the thick curve in Fig. 9.

In triaxial testing for anisotropic rocks with planes of weakness or pronounced fabric such as foliation in gneiss, the rock in which the preferred orientation of such anisotropy is perpendicular to the compressive stress direction has the highest strength and can be regarded as isotropic in the mechanical sense (e.g., Paterson, 1978; Jaeger and Cook, 1979). Yukutake and Shimada (1981) found in their triaxial testing on Kamioka gneiss that the compressive strengths are scattered against the confining pressure up to 240 MPa for samples with anisotropic foliation

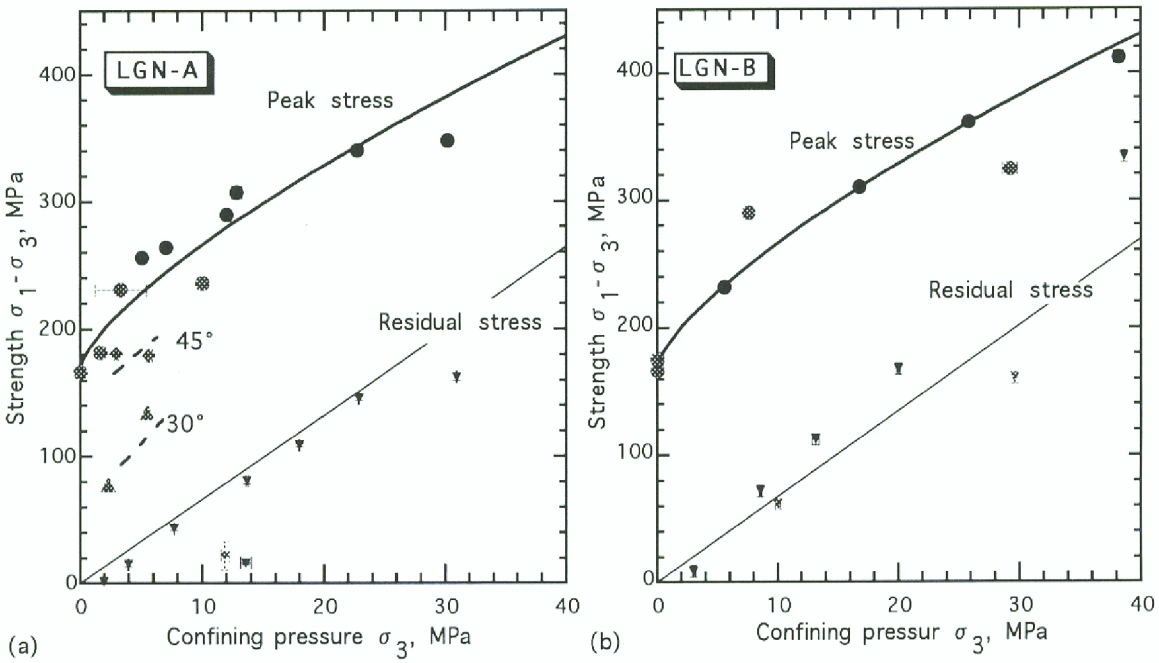

Fig. 9 Strength as a function of a confining pressure for LGNA (a) and LGNB (b). Stippled symbols indicate runs for the single-stage triaxial testing, and solid symbols for the multi failure state triaxial testing (MFSTT). Circles are the peak strengths ($LGNA_{\perp}$ in a). Triangles and diamonds are the peak strengths for $LGNA_{30}$ and $LGNA_{45}$, respectively. Small reverse triangles are the residual strengths. The thick curve and fine line are the estimated peak strength ($LGNA_{\perp}$ in a) and residual strength, respectively. Broken lines are the trends of peak strength for $LGNA_{30}$ and $LGNA_{45}$.

oriented at 45° to the compressive stress direction, with higher or lower value than for those at 90°. From this fact, they suggested the change in fracture mechanism at 240 MPa confining pressure (see also Shimada, 1992). Such a behavior was not observed in the present study, since runs for $LGNA_{45}$ as well as $LGNA_{30}$ were limited and confining pressure was in much lower level. The strength of these samples is shown only as a trend by broken lines in Fig. 9.

An interesting feature is observed in runs for $LGNA_{30}$ and $LGNA_{45}$, of which examples are shown in Fig. 10. The macroscopic fracture plane tends to be formed at orientation of 30° to the compressive stress direction in studied levels of confining pressure (cf. Table 2). $LGNA_{30}$ was fractured along the mylonitized foliation (Fig. 10a). This means that the foliation structure was planes of weakness, and one of them formed a macroscopic fracture plane, possibly according to the optimum condition of stress concentration for the used sample size. On the other hand, the fracture plane in $LGNA_{45}$ was zigzagged with macroscopic orientation of 25° - 30° (Fig. 10b), which consists of parts along foliation and their crossovers. This is considered that the influence of tendency of faulting oriented at 30° predominates over that of fault formation along an anisotropic weak plane throughout the sample, in accordance with the observation by Yukutake and Shimada (1981). According to them, the latter is anticipated to predominate over the former at higher confining

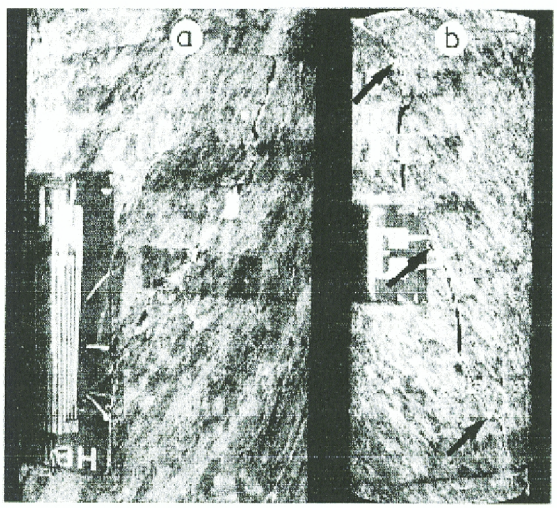

Fig. 10 Examples of fracture plane. a: $LGNA_{30}$ (run# LGN-15), note the fracture plane along foliation. b: $LGNA_{45}$ (run# LGN-16), note the zigzagged fracture plane that consists of parts along foliation (arrows) and their crossovers. The diameter of each sample is 20 mm, although a is enlarged.

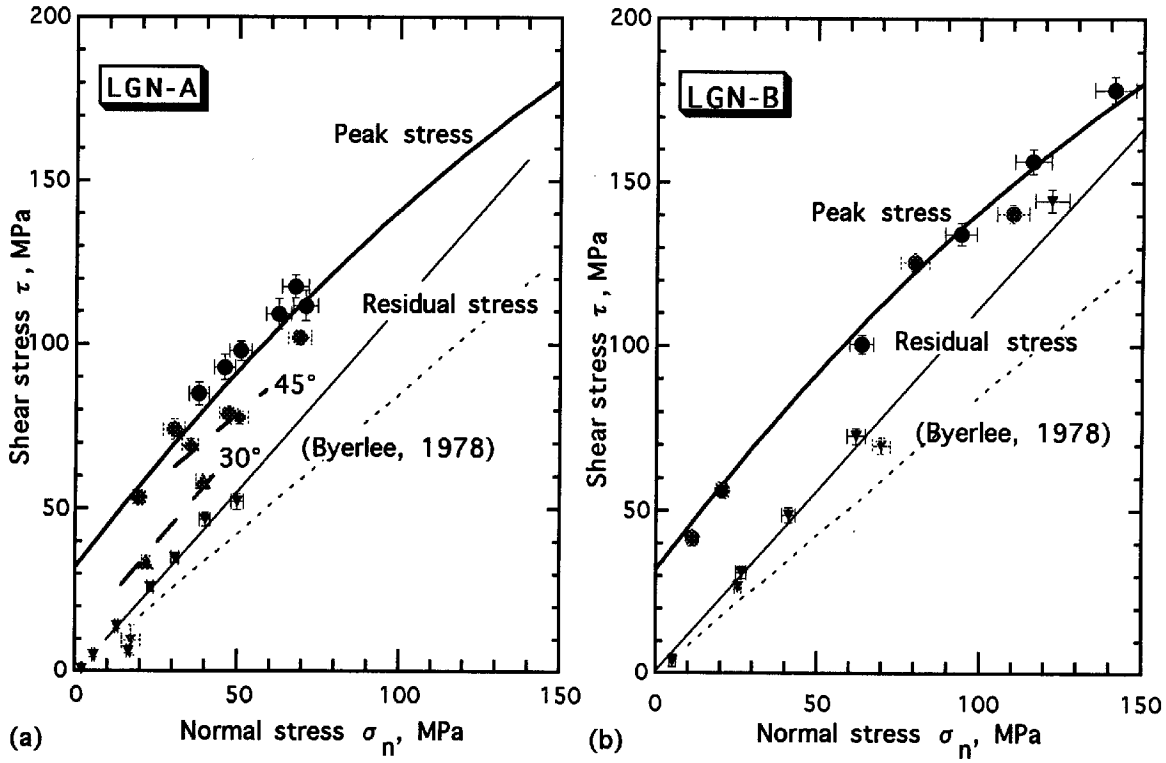

Fig. 11 Shear stress versus normal stress for peak and residual strengths, for LGNA (a) and LGNB (b). Symbols are the same as in Fig. 9. The dotted line is the frictional strength after Byerlee (1978).

pressure.

The normal stress and the shear stress for peak and residual strengths were calculated for the fracture plane using the following relationships:

$$\sigma_n = \sigma_3 + (\sigma_1 - \sigma_3)(1 - \cos 2\theta)/2$$

$$\tau = (\sigma_1 - \sigma_3)(\sin 2\theta)/2$$

where σ_n and τ are the normal stress and the shear stress for the plane with the fracture angle θ, and σ_3 and $\sigma_1 - \sigma_3$ are the confining pressure and the strength represented by differential stress, respectively. The obtained shear stress versus normal stress relation is shown in Fig. 11 (a for LGNA and b for LGNB), in which the Byerlee's (1978) relation for frictional strength of rocks is also shown. The obtained residual strength, which could be regarded as the frictional strength, is well fitted by a linear relationship:

$$\tau = 1.1\sigma_n$$

for $LGNA_{\perp}$ and LGNB. The slope, or the frictional coefficient, is 1.1, which is slightly larger than 0.85 by Byerlee (1978). Thus, the easiest sliding orientation is estimated at 21° to the compressive stress direction. It is conspicuous in Fig. 11 that the peak strength for $LGNA_{30}$, in which fracture occurs along a mylonitized foliation, is close to the residual strength. This suggests that the planes of foliation could easily slide as well as they form planes of weakness for fracture as discussed above. This would also accord with the presence of in situ macroscopic cracks along the foliation (see the left photograph in Fig. 3).

5. Concluding Remarks

Triaxial testing on two dry gneisses from the Lishan landslide slope was conducted at room temperature and a confining pressure up to 40 MPa. One, LGNA is from the upper bedrock of a fault plane that is considered to be a possible sliding surface, and the other, LGNB is from the lower bedrock. LGNA has an anisotropic structure of mylonitized foliation, while LGNB is isotropic. Both gneisses have a similar density of 2.7 Mg/m^3, while the porosity of LGNA is higher than of LGNB (Table 1). For LGNA, three samples, $LGNA_{\perp}$, $LGNA_{30}$ and $LGNA_{45}$ were prepared with foliation oriented at 90°, 30° and 45° to the compressive stress direction, respectively. $LGNA_{\perp}$ is regarded as isotropic in the mechanical sense.

$LGNA_{\perp}$ and LGNB were found to have the same

values of compressive strength and residual strength up to a confining pressure of 40 MPa (Fig. 9). The uniaxial compressive strength C_0 was 169.5 MPa. The compressive strength C was well represented by a power law of confining pressure σ_3:

$$C/C_0 = 1 + 4.34\,(\sigma_3/C_0)^{0.72}$$

and the residual strength was fitted by a linear relationship. The frictional coefficient was estimated at 1.1 from the residual strength (Fig. 11), corresponding to the easiest sliding orientation of 21° to the maximum compressive stress direction.

The compressive strength for $LGNA_{30}$ was close to the residual strength, suggesting that the plane of foliation could easily slide. The compressive strength for $LGNA_{45}$ was between those for $LGNA_{\perp}$ and $LGNA_{30}$.

For the bedrock sliding hypothesis for the mechanism of the Lishan landslide, sliding of a preexisting boundary should be considered, but not fracturing of either country rock, since the fracture strengths of both bedrocks are equal. This includes important factors to be solved, such as the interrelation among the direction of force acting at the expected landslide motion, the dip angle of the potential sliding plane and the orientation of foliation, which is out of scope of the present article. Considering higher porosity of the upper bedrock (LGNA) than of the lower one (LGNB), a high pore pressure could be possibly formed in the boundary between both bedrocks and the boundary could form a potential sliding surface.

Acknowledgments

I am greatly indebted to K. Sassa for his offering an opportunity to join the Japan-China Joint Research on Lishan Landslide and to sample rocks. I also thank all of Japanese and Chinese members of the 1994 joint research project, especially H. Sokobiki, R. Kitagawa and staff members in the Lintong Landslide Observatory for sampling rocks. I am indebted to R. Kitagawa and J. Liu for their petrological comments by observation of thin sections, to R. Koizumi for her help for modal analyses, and to T. Yanagidani, H. Kawakata, A. Nakagawa and S. Matsuo for their adjusting the measuring system and preparing experimental parts and apparatuses for triaxial testing.

References

Byerlee, J. (1978): Friction of rocks, *Pure Appl. Geophys.*, Vol. 116, pp. 615-626.

Hossaini, S. M. F. and Vutukuri, V. S. (1993): On the accuracy of multi-failure triaxial test for determination of peak and residual strengths of rocks, in *Geotechnical Instrumentation and Monitoring in Open Pit and Underground Mining*, edited by T. Szwedzicki, A. A. Balkema, Rotterdam, PP. 223-228.

ISRM (1983): Suggested methods for determining the strength of rock materials in triaxial compression: revised version, *Int. J. Rock Mech. Min. Sci. & Geomech. Abstr.*, Vol. 20, No. 6, pp. 283-290.

Jaeger, J. C. and Cook, N. G. W. (1979): *Fundamentals of Rock Mechanics, 3rd ed.*, Chapman and Hall, London, 593 p.

Kitagawa, R. (1997): Characteristic joint systems in the 2# tunnel at the Lishan slope, *Ann. DPRI Kyoto Univ.*, No. 40 (in press, in Japanese).

Kiyama, R. (1956): High pressure equipments in Abu-yama seismological observatory of Kyoto university, *Rev. Phys. Chem.*, Vol. 26, pp. 24-39.

Kovári, K. and Tisa, A. (1975): Multiple failure state and strain controlled triaxial tests, *Rock Mech.*, Vol. 7, pp. 17-33.

Lin, Z. (1989): Investigation and research on slope instability at Lishan (Lintong) historic scenic resort, *Proc. Jpn.-China Symp. Landslides and Debris Flows*, pp. 59-62.

Matsushima, S. (1960): On the deformation and fracture of granite under high confining pressure, *Bull. DPRI, Kyoto Univ.*, No. 36, pp. 11-20.

Ohnaka, M. (1973): The quantitative effect of hydrostatic confining pressure on the compressive strength of crystalline rocks, *J. Phys. Earth*, Vol. 21, pp. 125-140.

Paterson, M. S. (1978): *Experimental Rock Deformation — the Brittle Field*, Springer-Verlag, Berlin, 254 p.

Sassa, K. (1994): Prediction of landslide motion in Lishan (Huanqing Palace), Xian, China, *Landslide News*, No. 8, pp. 22-25.

Sassa, K. and Xie, Z. (Ed.) (1994): *Assessment of Landslide Hazards in Lishan (Yang-Que-Fe Palace), Xian, China*, Natural Hazard Reduction and Mitigation in the East Asia, Final Rept. Part 4 (Project E-2), 251 p.

Sassa, K., Fukuoka, H., Lee, J.-H., Shoaei, Z., Zhang, D., Xie, Z., Zeng, S. and Cao, B. (1994): Prediction of landslide motion based on the measurement of geotechnical parameters, in *Assessment of Landslide Hazards in Lishan (Yang-Que-Fe Palace), Xian, China*, edited by K. Sassa

and Z. Xie, Natural Hazard Reduction and Mitigation in the East Asia, Final Rept. Part 4 (Project E-2), pp. 13-47.

Shimada, M. (1992): Experimental earthquake prediction, *Earth Monthly*, Extra Vol., No. 4, pp. 168-173 (in Japanese).

Shimada, M. and Cho, A. (1990): Two types of brittle fracture of silicate rocks under confining pressure and their implications in the earth's crust, *Tectonophysics*, Vol. 175, No. 1-3, pp. 221-235.

Xie, Z., Chen, Y., Lin, Z. and Li, T. (1994): Lishan and investigation of the Lishan landslide, in *Assessment of Landslide Hazards in Lishan (Yang-Que-Fe Palace), Xian, China*, edited by K. Sassa and Z. Xie, Natural Hazard Reduction and Mitigation in the East Asia, Final Rept. Part 4 (Project E-2), pp. 49-91.

Yukutake, H. (1989): Fracturing process of granite inferred from measurements of spatial and temporal variations in velocity during triaxial deformations, *J. Geophys. Res.*, Vol. 95, No. B11, pp. 15639-15651.

Yukutake, H. and Shimada, M. (1981): On the selective fracture in anisotropic rocks, *J. Seismol. Soc. Jpn, Ser. 2*, Vol. 34, pp. 311-321 (in Japanese).

要　旨

中国華清池（驪山）地すべりの発生機構の一つとして，岩盤のクリープ運動が考えられている。有力なすべり面と考えられている断層を挟む2種の片麻岩（上盤をLGNA，下盤をLGNBと呼ぶ）が採取され，室温で封圧 40 MPa までの，圧縮強度と残留強度が測定された。両者の強度およびその封圧依存性は等しいことが判明した。LGNAは異方的な縞状構造が発達し，これに沿った巨視的なクラックが形成されている。一方，LGNBは巨視的には等方的である。これらの結果から，LGNA の方が空隙率が大きいことを考慮すると，2種の岩盤境界の間隙水圧が大きくなる可能性があり，この境界のすべりが予期されると考えられる。

キーワード：3軸試験，片麻岩，強度，地すべり，中国華清池（驪山）